

Received January 22, 2021, accepted February 13, 2021, date of publication February 18, 2021, date of current version February 26, 2021.

Digital Object Identifier 10.1109/ACCESS.2021.3060061

# Performance Verification of a Target Tracking System With a Laser Rangefinder

JIHOON LEE<sup>1</sup>, SUWON LEE<sup>1</sup>, YOUNGJUN LEE<sup>1</sup>, YOUDAN KIM<sup>1,2</sup>, (Senior Member, IEEE), YONGJUN HEO<sup>3</sup>, AND TAEDONG YOON<sup>3</sup>

<sup>1</sup>Department of Aerospace Engineering, Seoul National University, Seoul 08826, South Korea

<sup>2</sup>Institute of Advanced Aerospace Technology, Seoul National University, Seoul 08826, South Korea

<sup>3</sup>LIG Nex1 Company Ltd., Seongnam 13488, South Korea

Corresponding author: Youdan Kim (ydkim@snu.ac.kr)

This work was supported by LIG Nex1 Company Ltd.

**ABSTRACT** A target tracking system with a laser rangefinder is developed, and the performance of the developed system is verified by a numerical simulation and field tests. To develop the target tracking system, appropriate coordinate systems, motion models, and estimation methods are selected, and a range filter is designed to compensate for the measurement errors of the laser rangefinder. The range filter independently processes the range measurements so that the target filter continuously produces the target information. The entire target tracking system development process is described in detail to facilitate future work of a similar nature. A scenario-based Monte Carlo simulation is performed to compare the performances of various state estimation methods. Experimental tests involving a low-speed fishing boat and a drone are performed to verify the performance and effectiveness of the proposed scheme. A separate performance analysis program with a graphical user interface is developed to analyze the simulation and field test results.


**INDEX TERMS** Laser rangefinder, target tracking, state estimation.

## NOMENCLATURE

$\mathbf{p}_T^e$	Target position in ECEF coordinates
$\mathbf{v}_T^e$	Target velocity in ECEF coordinates
$\mathbf{p}_T^n$	Target position in navigation coordinates
$\mathbf{v}_T^n$	Target velocity in navigation coordinates
$\mathbf{p}_T^p$	Target position in platform coordinates
$\mathbf{p}_p^e$	Platform position in ECEF coordinates
$R_c^p$	DCM from camera to platform coordinates
$R_p^n$	DCM from platform to navigation coordinates
$R_n^e$	DCM from navigation to ECEF coordinates
$\phi, \lambda, h$	Geodetic latitude, longitude, and altitude
$\varphi, \theta, \psi$	Platform roll, pitch, and yaw angles
$A, E, R$	Azimuth, elevation, and range

## I. INTRODUCTION

Target tracking of a maneuvering target is one of the major problems in the field of defense and security. A target tracking system with various sensors, including a radar sensor, image sensors (e.g., an electro-optical camera), and a laser rangefinder (LRF), can be developed. In general, radar provides information on a target within a relatively wide field

The associate editor coordinating the review of this manuscript and approving it for publication was Rui-Jun Yan .

of view. However, a camera and an LRF are sometimes combined to obtain information about a target in a limited field of view with higher accuracy.

In this study, an LRF and electro-optical infrared image sensor are considered for the tracking of a maneuvering target. The LRF, which has been widely used for various applications [1], [2], uses the time-of-flight principle and measures the to-and-from travel time to determine the distance [3]. However, in addition to the typical additive noise signal, exceptional signal attributes exist, including false measurements in the range information from the LRF sensors. In the case of false measurements, the target signal may not be received because of the miss-hit (nonreflection) of the laser pulse, an occlusion by any obstacle during the mission, or an unexpected external light source, e.g., the sun. These attributes from the LRF sensor signals are characterized by actual data samples obtained from field experiments. Therefore, an additional filter for the LRF sensor should be designed to address the poor characteristics of the LRF and to handle exceptional signal attributes from the sensor [4].

A constant-gain filter and Kalman filter (KF) can be used for target tracking [5]. The alpha-beta filter (ABF) is a type of constant-gain filter that has been widely used because of its efficiency and easy implementation [6]. The KF was

first introduced in the 1960s and has been widely utilized to estimate the state information in various fields. The extended Kalman filter (EKF), which incorporates a linearization procedure, was developed for nonlinear systems. The unscented Kalman filter (UKF) is known to be more accurate than the EKF when the system has a strong nonlinearity because it does not compute the Jacobian at the expense of a larger computational load.

The target tracking problem can be understood as a nonlinear state estimation problem incorporating various coordinate systems. For example, target motion models, including the constant-velocity (CV) model and constant-acceleration (CA) model, are often described in a Cartesian coordinate system such as the earth-centered earth-fixed (ECEF) coordinate system. However, the measurement signals are obtained in the sensor coordinate system according to the measurement mechanism. Note that typical measurement signals are given as angles and ranges relative to the target, the transformation of which to a Cartesian coordinate system is nonlinear. Therefore, performing target tracking in different coordinate systems becomes a nontrivial problem. Rong Li *et al.* classified the tracking problem in various coordinate systems: i) tracking in mixed coordinates, ii) tracking in Cartesian coordinates, iii) tracking in sensor coordinates, and so on [7]. Mahapatra and Mehrotra proposed the mixed coordinate tracking of generalized maneuvering targets using the EKF [8]. Song *et al.* developed a suboptimal KF with a pseudo-measurement model by algebraically manipulating the original nonlinear measurement equation [9]. Aidala and Hammel utilized a modified polar coordinate system for bearing-only tracking [10].

In this study, a dual-loop filtering system is designed. A range filter is used to filter the signals from the LRF in the inner loop of the system. The range filter includes a signal processing scheme that can handle some exceptional cases to improve the signal quality and enrich the information extracted from the signals. Then, the filtered range signals and image sensor information are converted to the ECEF coordinate system. The state estimator for target tracking is designed in the ECEF coordinate system, which is used to construct the outer loop of the system. Various methods can be applied to the state estimator design, among which we consider the ABF, KF, EKF, cubature Kalman filter (CKF), and UKF in this study.

Our contributions are as follows. First, a novel range filter is designed to maintain the integrity of the range information used in the state estimator even under various exceptional signal attributes. Second, a framework for the development of a target tracking system is proposed that incorporates a scenario-based simulator and a performance analysis tool. The proposed framework covers the algorithm development, hardware implementation, and practical issues encountered during a field test of the target tracking system. The hardware implementation of the designed target tracking algorithm is described in detail, and the effectiveness of the target tracking system, verified via the field test, is discussed.

This paper is organized as follows. In Sec. II, the theoretical backgrounds of the coordinate systems, target motion models, measurement models, and state estimation methods are given. In Sec. III, the development process of the target tracking system is explained, followed by detailed design considerations for the range filter and the state estimator. In Sec. IV, the performance of the proposed target tracking algorithm is verified using the scenario-based simulator and performance analyzer. In Sec. V, the hardware implementation and experimental test results obtained using a ship and drone are presented. Finally, Sec. VI concludes this paper.

## II. PRELIMINARY

A target tracking filter can be designed in many different ways depending on the building blocks selected, which include the platform, hardware, and coordinate system. In this section, some basic elements of a target tracking filter and the underlying theories are briefly summarized. The coordinate systems, target motion models, measurement models, and state estimation methods are then discussed.

### A. COORDINATE SYSTEM

Transformation between different coordinate systems is required in the target tracking system. The coordinate systems used in the target tracking system are introduced below.

#### 1) WORLD GEODETIC SYSTEM 1984

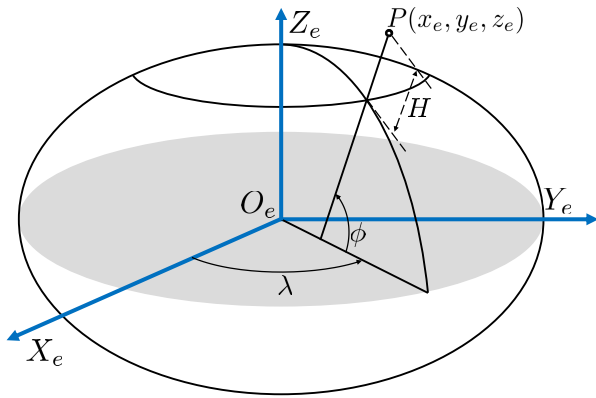
The World Geodetic System 1984 (WGS-84),  $O_w X_w Y_w Z_w$ , specifies each point uniquely in 3-D space using the geodetic latitude  $\phi$ , longitude  $\lambda$ , and altitude  $H$ , as shown in Fig. 1a. Longitude is defined as the angle in the equatorial plane between the  $O_w X_w$  vector and  $O_w Y_w$  vector. Geodetic latitude is defined as the angle between the equatorial plane and the surface normal at a certain point on an ellipsoid. Altitude is defined as the distance from the point to the reference ellipsoid tangent plane. In this study, the global positioning system (GPS) locations of the platform and the target are obtained, and these locations are represented in the WGS-84. The target GPS information is available only in the test environment.

#### 2) EARTH-CENTERED EARTH-FIXED COORDINATE SYSTEM

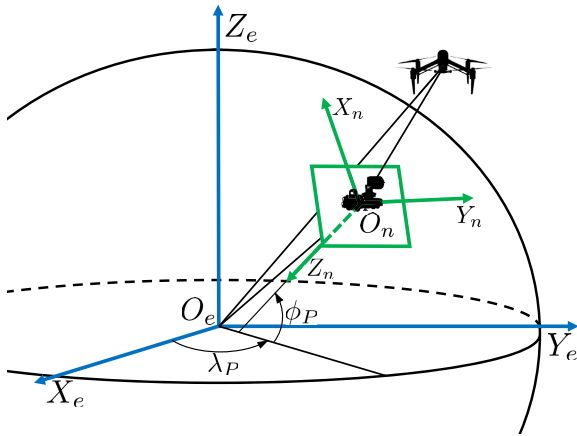
The origin of the ECEF coordinate system ( $O_e X_e Y_e Z_e$ ) is located at the center of mass of the Earth. The axes of the ECEF system are fixed with respect to the Earth's surface. The target tracking filter estimates the target states in the ECEF coordinate system.

#### 3) NAVIGATION COORDINATE SYSTEM

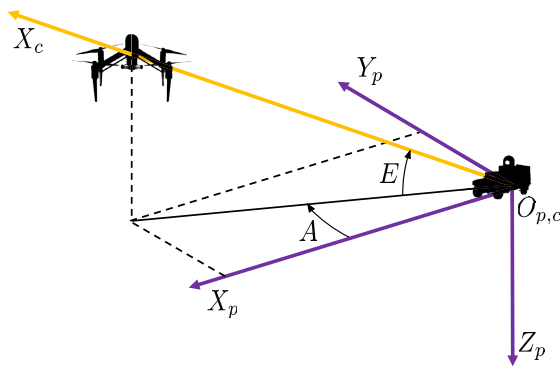
The navigation coordinate system ( $O_n X_n Y_n Z_n$ ) has its origin at the center of mass of the platform ( $O_n$ ), and the axes are aligned with the north ( $O_n X_n$ ), east ( $O_n Y_n$ ), and down ( $O_n Z_n$ ) directions, as shown in Fig. 1b. In this study, the target velocity is represented in the navigation coordinate system. Because the target tracking filter estimates the target velocity in the ECEF coordinate system, coordinate transformation



(a) Schematic diagram of the WGS-84 and ECEF coordinate systems



(b) Schematic diagram of the ECEF and navigation coordinate systems



(c) Schematic diagram of the platform and camera coordinate systems

**FIGURE 1. Schematic diagrams of the coordinate systems.**

from the ECEF system to the navigation coordinate system is required.

#### 4) PLATFORM COORDINATE SYSTEM

The platform coordinate system ( $O_p X_p Y_p Z_p$ ) shares its origin with that of the navigation coordinate system ( $O_p$ ), and

the x-axis ( $O_p X_p$ ) points toward the head of the platform, as shown in Fig. 1c. The z-axis ( $O_p Z_p$ ) points downward, and the y-axis ( $O_p Y_p$ ) is aligned with the right side of the platform. The platform coordinate system axes are obtained through a 3-2-1 Euler angle rotation from the NED coordinate system axes. The acceleration, attitude, and angular rate of the platform measured by the inertial navigation system (INS) mounted on the platform are provided in this coordinate system.

#### 5) CAMERA COORDINATE SYSTEM

The camera coordinate system ( $O_c X_c Y_c Z_c$ ) has its origin  $O_c$  at the center of the sensor axes. The x-axis ( $O_c X_c$ ) points toward the target. The camera coordinate system axes are obtained through a 3-2-1 Euler angle rotation from the platform coordinate system axes. The LRF is oriented in the same direction as the x-axis of the camera coordinate system.

### B. TARGET MOTION MODEL

In this section, several fundamental target motion models are briefly explained. The models can be used in single-model or multimodel algorithms. In this study, the target is treated as a point mass. A continuous-time state-space model describes the target motion, and the target motion model is described in ECEF coordinates. A discrete-time linear model can be obtained through linearization and discretization as

$$\mathbf{x}_{k+1} = F_k \mathbf{x}_k + G_k \mathbf{w}_k \quad (1)$$

where  $\mathbf{x}_k$  is the target state,  $\mathbf{w}_k$  is the process noise,  $F_k$  is the state transition matrix,  $G_k$  is the process noise influence gain, and the subscript  $k$  denotes the related time step. The process noise is assumed to be a zero-mean white Gaussian sequence, i.e.,  $\mathbf{w}_k \sim \mathcal{N}(0, Q_k)$ , where  $Q_k$  is the process noise covariance.

Various simple low-order motion models can be successfully applied to the tracking of a wide range of targets with moderate maneuverability. Therefore, in this study, a CV model and a CA model are considered.

#### 1) CONSTANT-VELOCITY MODEL

The CV model assumes that the target has CV motion (including stationary motion) with zero-mean white Gaussian acceleration noise. This model can be used for the tracking of targets with relatively steady (zero-acceleration) motion, which can be formulated as

$$\mathbf{x}_k = F_{CV} \mathbf{x}_{k-1} + G_{CV} \mathbf{w}_{k-1} \quad (2)$$

where  $\mathbf{x}_k = [x, \dot{x}, y, \dot{y}, z, \dot{z}]^T$  and

$$F_{CV} = \begin{bmatrix} \Phi_{CV} & O_{2 \times 2} & O_{2 \times 2} \\ O_{2 \times 2} & \Phi_{CV} & O_{2 \times 2} \\ O_{2 \times 2} & O_{2 \times 2} & \Phi_{CV} \end{bmatrix} \quad (3)$$

$$G_{CV} = \begin{bmatrix} \Gamma_{CV} & O_{2 \times 1} & O_{2 \times 1} \\ O_{2 \times 1} & \Gamma_{CV} & O_{2 \times 1} \\ O_{2 \times 1} & O_{2 \times 1} & \Gamma_{CV} \end{bmatrix} \quad (4)$$

with

$$\Phi_{CV} = \begin{bmatrix} 1 & \Delta t \\ 0 & 1 \end{bmatrix}, \quad \Gamma_{CV} = \begin{bmatrix} \frac{\Delta t^2}{2} \\ \Delta t \end{bmatrix} \quad (5)$$

## 2) CONSTANT-ACCELERATION MODEL

The CA model assumes that the target has CA motion (including CV motion) with zero-mean white Gaussian jerk noise. This model can be used for the tracking of moderately maneuvering targets, which can be formulated as

$$\mathbf{x}_k = F_{CA}\mathbf{x}_{k-1} + G_{CA}\mathbf{w}_{k-1} \quad (6)$$

where  $\mathbf{x}_k = [x, \dot{x}, \ddot{x}, y, \dot{y}, \ddot{y}, z, \dot{z}, \ddot{z}]^T$  and

$$F_{CA} = \begin{bmatrix} \Phi_{CA} & O_{3 \times 3} & O_{3 \times 3} \\ O_{3 \times 3} & \Phi_{CA} & O_{3 \times 3} \\ O_{3 \times 3} & O_{3 \times 3} & \Phi_{CA} \end{bmatrix} \quad (7)$$

$$G_{CA} = \begin{bmatrix} \Gamma_{CA} & O_{3 \times 1} & O_{3 \times 1} \\ O_{3 \times 1} & \Gamma_{CA} & O_{3 \times 1} \\ O_{3 \times 1} & O_{3 \times 1} & \Gamma_{CA} \end{bmatrix} \quad (8)$$

with

$$\Phi_{CA} = \begin{bmatrix} 1 & \Delta t & \frac{\Delta t^2}{2} \\ 0 & 1 & \Delta t \\ 0 & 0 & 1 \end{bmatrix}, \quad \Gamma_{CA} = \begin{bmatrix} \frac{\Delta t^3}{6} \\ \frac{\Delta t^2}{2} \\ \Delta t \end{bmatrix} \quad (9)$$

## C. MEASUREMENT MODEL

The following nonlinear measurement equation is considered:

$$\mathbf{z}_k = \mathbf{h}(\mathbf{x}_k) + \mathbf{v}_k \quad (10)$$

where  $\mathbf{z}_k = [A, E, R]^T$  is the measurement,  $\mathbf{v}_k$  is the measurement noise, and  $\mathbf{h}(\cdot)$  is the measurement function. In this study, the measurement consists of the azimuth  $A$ , elevation  $E$ , and range  $R$ , which can be represented as

$$A = \arctan\left(\frac{y^p}{x^p}\right) \quad (11)$$

$$E = \arctan\left(\frac{z^p}{\sqrt{(x^p)^2 + (y^p)^2}}\right) \quad (12)$$

$$R = \sqrt{(x^p)^2 + (y^p)^2 + (z^p)^2} \quad (13)$$

where  $[x^p, y^p, z^p]^T$  is the target position in the platform coordinate system. The measurements are assumed to be subject to zero-mean white Gaussian noise, i.e.,  $\mathbf{v}_k \sim \mathcal{N}(0, R_k)$ , where  $R_k = \text{diag}(\sigma_A^2, \sigma_E^2, \sigma_R^2)$ . To apply a linear filter, the measurement vector is transformed into a position vector in the ECEF coordinate system. That is, the following linear measurement equation is used:

$$\mathbf{z}_k = H_k \mathbf{x}_k + \mathbf{v}_k \quad (14)$$

where  $\mathbf{z}_k = [x, y, z]^T$  and  $H_k$  is a measurement matrix.

## D. STATE ESTIMATION

State estimation is very important in target tracking. Therefore, a state estimation method should be carefully selected based on the characteristics of the target and measurement sensors. In this study, the ABF, KF, and EKF are considered.

### 1) ALPHA-BETA FILTER

The ABF is a constant-gain state observer. It is widely used in target tracking systems mainly because it does not require a system model. The prediction step of the ABF can be described as [11]

$$\bar{\mathbf{p}}_k = \bar{\mathbf{p}}_{k-1} + \Delta t \bar{\mathbf{v}}_{k-1} \quad (15)$$

$$\bar{\mathbf{v}}_k = \bar{\mathbf{v}}_{k-1} \quad (16)$$

where  $\bar{\mathbf{p}}_k$  and  $\bar{\mathbf{v}}_k$  denote the predicted (a priori) position and velocity in the ECEF coordinate system, respectively, and  $\Delta t$  is a time interval of the estimation. The correction step of the ABF can be described as

$$\hat{\mathbf{p}}_k = \bar{\mathbf{p}}_k + \alpha \tilde{\mathbf{r}}_k \quad (17)$$

$$\hat{\mathbf{v}}_k = \bar{\mathbf{v}}_k + \frac{\beta}{\Delta t} \tilde{\mathbf{r}}_k \quad (18)$$

where  $\hat{\mathbf{p}}_k$  and  $\hat{\mathbf{v}}_k$  denote the corrected (a posteriori) estimates of the position and velocity, respectively,  $\alpha$  and  $\beta$  are constant gains for the position and velocity correction, respectively, and  $\tilde{\mathbf{r}}_k$  is the measurement residual, defined as the difference between the measured position value and the predicted position value.

However, an alpha-beta-gamma filter (ABGF) provides smoothed estimates of the position, velocity, and acceleration. The prediction step of the ABGF can be described as [11]

$$\bar{\mathbf{p}}_k = \bar{\mathbf{p}}_{k-1} + \Delta t \bar{\mathbf{v}}_{k-1} + \frac{\Delta t^2}{2} \bar{\mathbf{a}}_{k-1} \quad (19)$$

$$\bar{\mathbf{v}}_k = \bar{\mathbf{v}}_{k-1} + \Delta t \bar{\mathbf{a}}_{k-1} \quad (20)$$

$$\bar{\mathbf{a}}_k = \bar{\mathbf{a}}_{k-1} \quad (21)$$

where  $\bar{\mathbf{a}}_k$  denotes the predicted acceleration. The correction step of the ABGF can be described as

$$\hat{\mathbf{x}}_k = \bar{\mathbf{x}}_k + \alpha \tilde{\mathbf{r}}_k \quad (22)$$

$$\hat{\mathbf{v}}_k = \bar{\mathbf{v}}_k + \Delta t \bar{\mathbf{a}}_k + \frac{\beta}{\Delta t} \tilde{\mathbf{r}}_k \quad (23)$$

$$\hat{\mathbf{a}}_k = \bar{\mathbf{a}}_k + \frac{2\gamma}{\Delta t^2} \tilde{\mathbf{r}}_k \quad (24)$$

where  $\gamma$  is the constant gain for the acceleration correction.

### 2) KALMAN FILTER

The KF also consists of two steps: a prediction step (time update) and a correction step (measurement update). In the prediction step, the state and covariance are updated according to the target motion model as

$$\bar{\mathbf{x}}_k = F_{k-1} \bar{\mathbf{x}}_{k-1} \quad (25)$$

$$\bar{P}_k = F_{k-1} \bar{P}_{k-1} F_{k-1}^T + G_{k-1} Q_{k-1} G_{k-1}^T \quad (26)$$

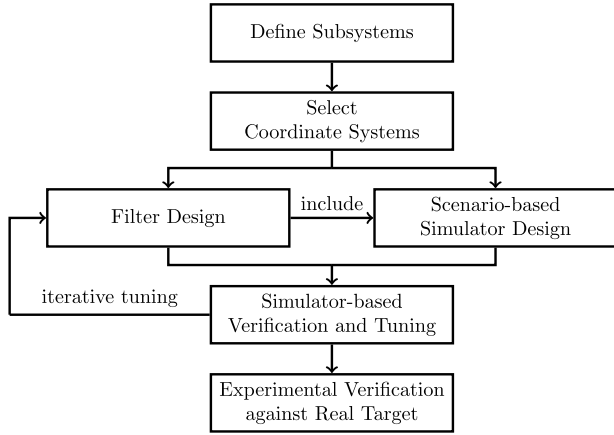


FIGURE 2. Flow chart of the development process.

where  $\bar{P}_k$  denotes the predicted error covariance and  $Q_k$  is the process noise covariance. In the correction step, the state and error covariance are updated according to the prefit residual  $\mathbf{r}_k = \mathbf{z}_k - H_k \bar{\mathbf{x}}_k$  as

$$\hat{\mathbf{x}}_k = \bar{\mathbf{x}}_k + K_k \mathbf{r}_k \quad (27)$$

$$\hat{P}_k = \bar{P}_k - K_k S_k K_k^T \quad (28)$$

where  $\hat{P}_k$  denotes the corrected error covariance and the prefit residual covariance  $S_k$  and KF gain  $K$  are calculated as

$$S_k = H_k \bar{P}_k H_k^T + R_k \quad (29)$$

$$K_k = \bar{P}_k H_k^T S_k^{-1} \quad (30)$$

### 3) EXTENDED KALMAN FILTER

The EKF is widely used for the state estimation of a nonlinear system. In the prediction step, the state and the covariance are updated using a Jacobian of the state transition function as

$$\bar{\mathbf{x}}_k = \mathbf{f}(\bar{\mathbf{x}}_{k-1}) \quad (31)$$

$$\bar{P}_k = F_{k-1} \bar{P}_{k-1} F_{k-1}^T + G_{k-1} Q_{k-1} G_{k-1}^T \quad (32)$$

where  $\mathbf{f}(\cdot)$  is a state transition function and  $F_{k-1} = \left. \frac{\partial \mathbf{f}}{\partial \mathbf{x}} \right|_{\bar{\mathbf{x}}_{k-1}}$ .

In the correction step, the state and the covariance are updated as

$$\hat{\mathbf{x}}_k = \bar{\mathbf{x}}_k + K_k \mathbf{r}_k \quad (33)$$

$$\hat{P}_k = \bar{P}_k - K_k S_k K_k^T \quad (34)$$

where  $\mathbf{r}_k = \mathbf{z}_k - \mathbf{h}(\bar{\mathbf{x}}_k)$  and

$$S_k = H_k \bar{P}_k H_k^T + R_k \quad (35)$$

$$K_k = \bar{P}_k H_k^T S_k^{-1} \quad (36)$$

with  $H_k = \left. \frac{\partial \mathbf{h}}{\partial \mathbf{x}} \right|_{\bar{\mathbf{x}}_k}$ .

## III. SYSTEM DEVELOPMENT

In this section, the overall development of the target tracking system is described. The design considerations for the range filter and the state estimator are also explained.

### A. OVERALL SYSTEM DEVELOPMENT PROCESS

The overall development process is depicted in Fig. 2. In the first step, all the subsystems in the target tracking system are defined, including the sensors, platforms, and targets. In this study, an LRF and image sensors are considered. Various platforms and targets, i.e., stationary and moving objects, including cars, ships, and flight vehicles, can be considered.

*Remark: Various types of platforms and targets must be considered because the maneuvering characteristics are different for each. For example, cars and ships maneuver only on the surface of the Earth, while airplanes can maneuver in three-dimensional space. Ships may have irregular swaying depending on the state of the sea, which does not occur for ground-based vehicles. The cruising speeds for each are also different.*

In the second step, appropriate coordinate systems are selected, and the transformation and relationship between each of the coordinate systems are clarified. Detailed mathematical explanations of the various coordinate systems and their transformations can be found in the Appendix. In this study, the WGS-84 is selected to validate the developed system through hardware experiments and numerical simulations. The NED coordinate system, the center of which is fixed at the sensor platform, and the camera coordinate system, the x-axis of which is pointed toward the target position, are also considered.

In the third step, filters for target tracking are designed for several coordinate systems. In this study, a range filter is formulated for the camera coordinate system, and a state estimator for position tracking of a target is formulated for the ECEF coordinate system.

Now, let us describe the development of the scenario-based simulator. First, various scenarios of the target and platform are defined, and the filters are incorporated into the simulator. The simulator computes the position and velocity of the platform and target in the WGS-84 coordinate system and the relative geometry. True signals are obtained from the relative geometry, and the sensor measurement signal is obtained from the true signals with noise. In this study, an LRF and image sensors are considered, and therefore, the measurement signal attributes of the LRF and image sensors are mathematically modeled. Then, the performance of the tracking filter is evaluated. Note that the parameters of the filter should be tuned based on the considered scenarios. The appropriate filter parameters may have different values depending on the scenarios considered, thus yielding satisfactory performance for each scenario. In this study, an analysis tool with a graphic user interface (GUI) is developed and utilized to verify the designed filter and to carry out gain tuning. An explanation of the development of the scenario-based simulator and the GUI-based performance analyzer is given in Sec. IV. Finally, performance verification through hardware experiments is conducted. The performance of the developed target tracking system is verified against the actual motion of the target. In this study, moving targets, including a ship and a drone, are used for the field test. The hardware

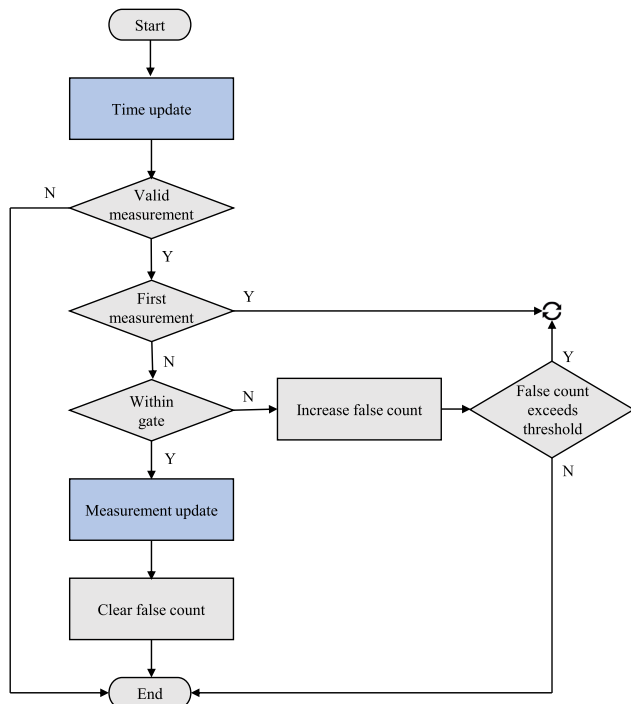


FIGURE 3. Flow chart of the range filtering algorithm.

implementation and performance verification are described in Sec. V.

## B. TARGET TRACKING FILTER DESIGN PROCESS

The target tracking filter is designed in two parts: the range filter and the state estimator. The range filter processes the raw range measurements and hands over the filtered range to the state estimator. Then, the state estimator estimates the target information in the ECEF coordinate system based on the processed range with the azimuth and elevation information given.

### 1) RANGE FILTER

The distance from the platform equipped with the target tracking system to the target is measured using an LRF, which is vulnerable to various error sources and noise. Data processing routines must generate consistent range information from the raw data of the range measurements. In this study, the range filter is designed by combining a 1-dimensional linear KF with a set of data processing algorithms. The CV, CA, and CJ models are considered for the target model.

The flow chart of the range filter is shown in Fig. 3. At every time step, the range filter propagates the range estimate according to the target model. The data processing procedure to exclude invalid data is as follows. When a range measurement is received by the LRF, the filter decides whether or not to perform correction based on an assessment of the received signal. If the received measurement is out of the sensor detection limit, then the corresponding step is immediately stopped, and the time-updated range is used

without a measurement update. If the received signal is a valid signal for the first time after the last reset, then the filter is reset with the current measurement. Otherwise, the filter judges whether the measurement is from the target or clutter by applying a gate based on the current estimate of the range estimation error covariance. If the valid measurement is found to be outside the gate, then the filter records the elapsed time since the last target measurement. If the target measurement has not been received over the prescribed threshold time, then the filter determines that the target of interest has changed and initializes the estimation process according to the new object. The measurement update is performed only when all the aforementioned criteria are met.

Four decision stages are carried out to address outliers in the LRF measurement, as shown in Fig. 3. First, the filter regards the measurement as valid if it has a nonzero positive value within the maximum operational range of the LRF (20 km). Second, the filter state initialized with a temporary range value is immediately replaced with the newly available valid measurement. This stage is included because use of a filter is necessary for system operation even if no available range measurement exists. In addition, the dummy range value does not need to be preserved once a valid measurement is received. Third, the range filter forms a gate with varying width. The gate is used to address the uncertainty in the target motion, and the width is determined based on the knowledge of the target maneuverability. In this study, three techniques are used to compute the gate width: i) use of a fixed width, ii) multiplication of the maximum target speed by the time elapsed since the last measurement, and iii) estimation of the error covariance of the range filter with a constant multiplier (e.g.,  $3\sigma$ ). The final stage reflects the design requirement that the filter should be able to change the target to be tracked automatically if the measurement occurs outside the gate for a certain period of time (12.5 s in the following examples), which is different from the standard data association technique. With these four decision stages combined with the standard KF, the range filter maintains consistent tracking of the target even under temporary target loss.

### 2) STATE ESTIMATOR

The state estimator estimates the target states in the ECEF coordinate system based on the range information received from the range filter. In this study, both the linear and nonlinear state estimators are considered. In the linear filter, the measurements in the sensor coordinate system are transformed into the target position in the ECEF coordinate system. Then, the filter estimates the target states based on the system model. On the other hand, in the nonlinear filter, the nonlinear measurement function is used directly. Even though the target motion model may be nonlinear, only linear motion models are considered in this study. The state estimator updates the estimates through two steps: prediction and correction. A detailed explanation of the linear and nonlinear filters considered in this study was given in the previous section.

**TABLE 1.** Selection options for the scenario panel of the performance analyzer.

Item	Option
Platform	Stationary, Car, Ship
Target	Stationary, Car, Ship, Airplane
Direction	Inbound, Outbound, Cross, In-Cross, Out-Cross
Altitude	Stationary, Ascending, Descending
Filter	ABF, ABGF, CV-KF, CA-KF, CV-EKF, CA-EKF

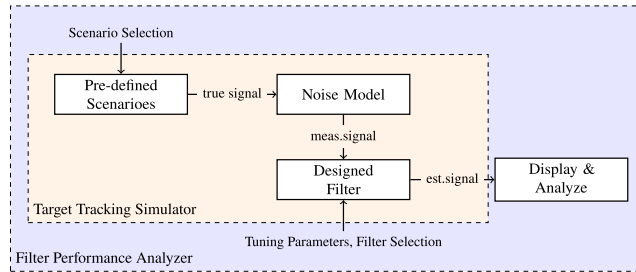


**FIGURE 4.** Target tracking simulator and performance analyzer.

#### IV. SCENARIO-BASED NUMERICAL SIMULATION

In this section, a scenario-based target tracking simulator and a performance analysis tool are developed for verification of the proposed target tracking system. The purpose and effectiveness of the simulator and tool in the development process are discussed in detail.

##### A. SIMULATOR AND ANALYSIS TOOL DEVELOPMENT

The simulator can consider various scenarios, i.e., trajectories, of the target and the platform equipped with the target tracking system. The true signals are computed from the relative kinematic geometry considering the trajectories in the simulator, which are processed through a noise model to generate the measurement signals. In the noise model, the true signals are corrupted with zero-mean Gaussian noise. Note that a random mask is applied to the range signal. The range filter handles the corrupted range signal using a filtering algorithm and provides the processed signal, which is used in the state estimator. The state estimation filters are embedded in the simulator, and the filtering is processed to obtain estimates of the target information. Finally, the simulator is connected to the performance analyzer. In this study, a performance analyzer with a GUI is developed to facilitate performance analysis and filter tuning. The GUI-based performance analyzer helps the user to tune the filter design parameters. The whole process of the target tracking simulator and the performance analyzer is shown in Fig. 4.

The simulator and the analysis tool are developed in the MATLAB R2020a environment. Fig. 5 shows the filter performance analyzer GUI window developed using the

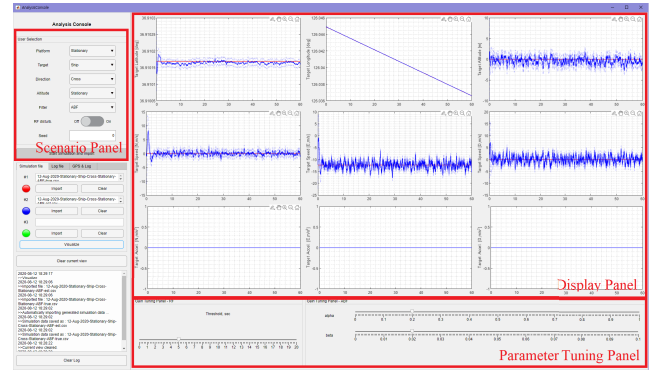


**FIGURE 5.** Performance analyzer GUI.

MATLAB App Designer. In the *scenario panel* of the GUI, the motions of the target and platform can be selected. Types and directions of the target and platform can also be selected on the same panel. The state estimation filters can be selected in the *scenario panel*. The selection options in the *scenario panel* are summarized in Table 1.

The tuning of the filter parameter is conducted in the *parameter tuning panel*. After the filter type is selected in the *scenario panel*, the *parameter tuning panel* automatically shows the corresponding tunable parameters for the selected filter. Finally, the simulation is conducted for the selected scenario and parameter settings.

One of the most important steps in using the performance analyzer is to select the most appropriate filter type and parameters for a particular target of interest. First, the pros and cons of each filtering method should be understood. For example, nonlinear filters usually outperform linear filters when it comes to nonlinear motion models at the cost of higher computational complexity, and higher-degree motion models are preferred to track a target with high maneuverability. If use of a specific target motion model is difficult, then the ABF can be used, which does not require a detailed system model. Second, the filter parameters are adjusted to make the best use of the selected filter type; this process is conducted typically in an experimental manner or on the basis of the engineer’s experience. For example, the ABF parameters can be treated as step sizes, or they can be related to a steady-state KF with the following formula [12]:

$$\lambda = \frac{\sigma_w T^2}{\sigma_v} \tag{37}$$

$$r = \frac{4 + \lambda - \sqrt{8\lambda + \lambda^2}}{4} \tag{38}$$

$$\alpha = 1 - r^2 \tag{39}$$

$$\beta = 2(2 - \alpha) - 4\sqrt{1 - \alpha} \tag{40}$$

The optimal parameters can also be calculated in a similar way [12]. On the other hand, the tuning process of KFs consists of two aspects. The measurement noise level can be adopted directly from the sensor sheets, and the process noise level should be increased in proportion to the degree of

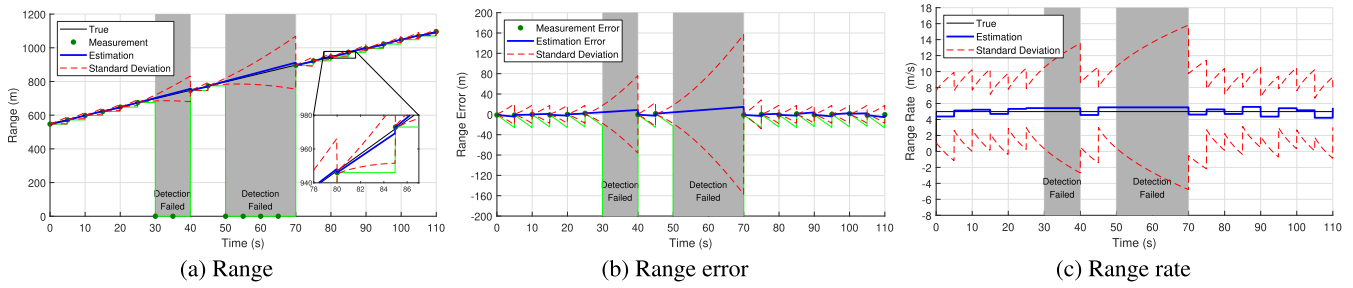


FIGURE 6. Range filter response - Outbound case.

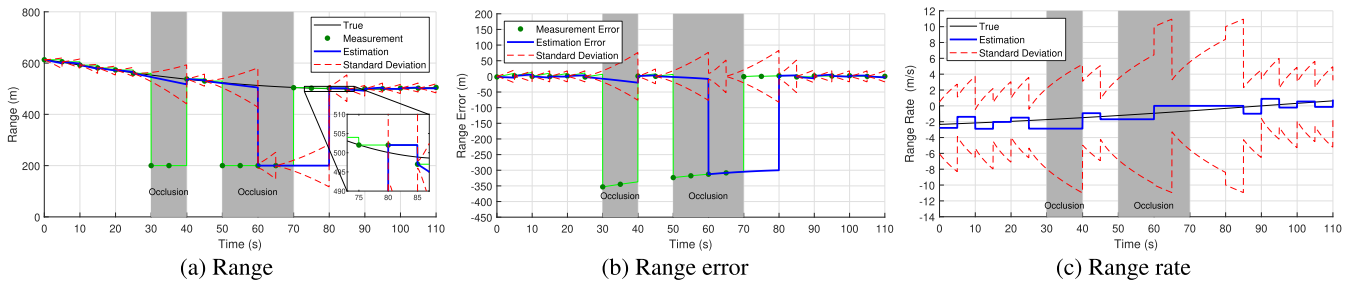


FIGURE 7. Range filter response - Cross case.

maneuverability of the target. Larger values are usually used for the process noise when precise knowledge of the degree of target maneuverability is not available.

The full simulation result is automatically saved in comma-separated value (CSV) format and displayed in the *display panel*. The *display panel* shows the position, velocity, and acceleration estimates from the simulation result. Two or more different simulation results in the CSV format can be imported and displayed simultaneously, which enables comparative analysis.

**B. TRACKING SIMULATION RESULT**

Various scenarios can be considered using the developed simulator. In this section, among many possible simulation scenarios, three cases are selected and discussed: i) outbound, ii) inbound, and iii) cross motion of the target. A ship-type target (i.e., constant altitude) with a speed of 5-7 m/s is considered in the simulation, where the platform is stationary.

**1) RANGE FILTER VERIFICATION**

In this section, the range filter simulation results are presented. The sensor model includes application of a disturbing mask to the true range signal that mimics the measurement failure in the LRF sensor. The range measurement is generated every 5 s throughout the simulation. Note that the considered LRF has three operational frequencies from 0.2 Hz to 5 Hz, but the lowest frequency is used in normal operational mode considering the life span of the equipment. The measurement is corrupted by white Gaussian noise with a standard deviation of 1 m. Then, the range measurement is rounded off to the nearest integer, as in the real hardware

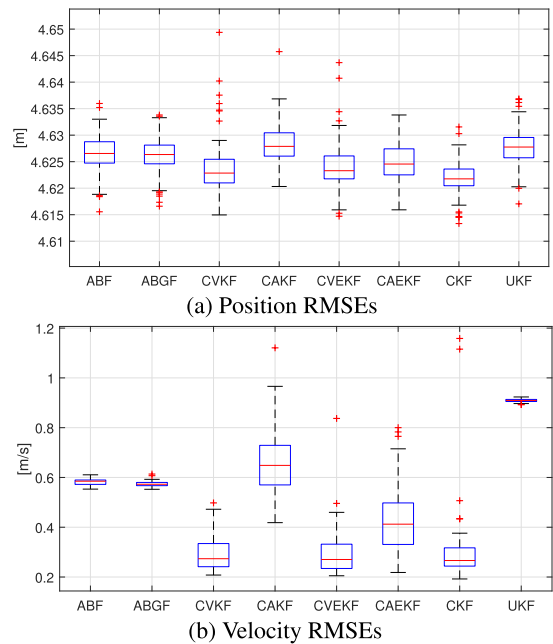


FIGURE 8. Position and velocity RMSEs of different filters.

system considered in this study. Finally, the zero range is overwritten on the generated measurement when the LRF misses the target, and the 200 m range is overwritten in the case of occlusion, assuming the situation where an unexpected object comes in between the observation device and the target. The filtering results are shown in Figs. 6 and 7.

Fig. 6 shows the exception handling result of cases of LRF failure. The scenario of Fig. 6 is the outbound case



TABLE 2. Summary of the Monte Carlo simulation results.

Filter Type	ABF	ABGF	CV-KF	CA-KF	CV-EKF	CA-EKF	CKF	UKF
Avg. pos. estimation RMSE (m)	4.6270	4.6260	4.6238	4.6284	4.6245	4.6247	4.6300	4.6278
Avg. vel. estimation RMSE (m/s)	0.5823	0.5738	0.2974	0.6596	0.2951	0.4261	0.2965	0.9089

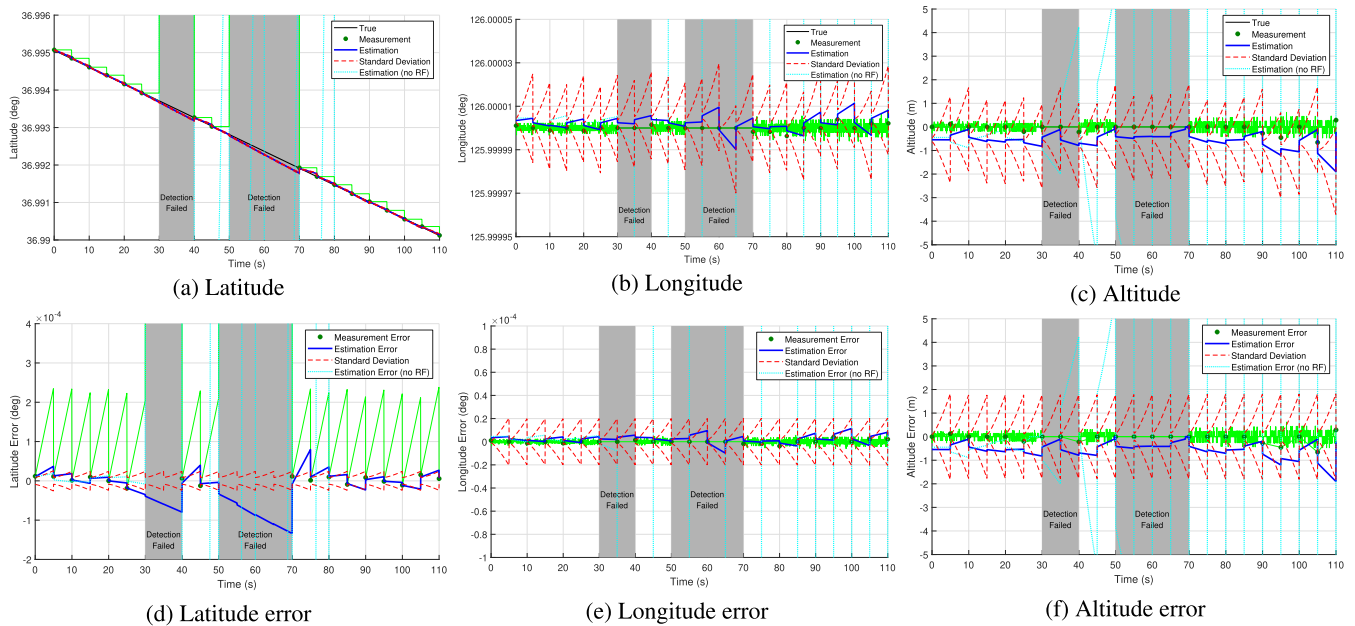


FIGURE 9. State estimator simulation results under detection failure - Outbound case.

and has two intervals of LRF failure, i.e., the [30, 40] s and [50, 70] s intervals, as the disturbing mask. When the LRF fails to detect the target, the range measurement output becomes zero, as shown in Fig. 6. Note that when the LRF fails to obtain the distance data, the range filter propagates the model and does not conduct the measurement update. Consequently,  $\sigma$  increases during the time interval of the LRF failure.

Fig. 7 shows the exception handling result of occlusion. The scenario of Fig. 7 is the cross case and has two intervals of occlusion (blocking), i.e., the [30, 40] s and [50, 70] s intervals, as the disturbing mask. In the occlusion case, it is assumed that an obstacle occludes the target at a distance of 200 m from the platform. The difference between the LRF failure case and the occlusion case is the allowance of the selection of different targets. The range filter is designed to endure for the predefined time during which occlusion occurs, i.e., the large discrepancy between the new measurement and the previous measurement. However, if the LRF measures an obstacle over the predefined endurance time, then the filter automatically resets and considers it a new target. In the simulation, the endurance time is set to 12.5 s. Note that in the first occlusion of [30, 40] s, the filter still follows the target and propagates the estimated signal. However, in the second occlusion of [50, 70] s, the filter resets and changes the target because the time interval is longer than the predefined endurance time.

## 2) STATE ESTIMATOR VERIFICATION

Once the range filter design process is finished, the performance of the state estimator should also be verified. The performance analyzer helps the user tune the filter parameters. The LRF signal attributes (disturbing mask) are not applied in the analysis of the state estimator. In this study, the ABF, ABGF, CV-KF, CA-KF, CV-EKF, CA-EKF, CKF, and UKF are considered.

After the parameters of each filter are tuned, 100 Monte Carlo simulations are conducted for the performance evaluation of these filters. The Monte Carlo simulation results are summarized in Table 2 and Fig. 8. The average root mean square errors (RMSEs) of the KF and EKF are smaller than those of the ABF and ABGF. This result is reasonable because the actual target movement is similar to that of the CV model. The EKF is expected to show more robust performance throughout various situations.

Example simulation cases of the filtering result in the WGS-84 with the CV-EKF are shown in Figs. 9 and 10. Similar to the range filter tuning results in Figs. 6 and 7, the LRF failure and occlusion cases are considered for the outbound scenario and the cross scenario.

## 3) TRACKING PERFORMANCE COMPARISON

We carry out a comparative study in two ways. First, a Monte Carlo simulation is performed using 8 different filters for the ‘cross’ case, where exceptional signal attributes other

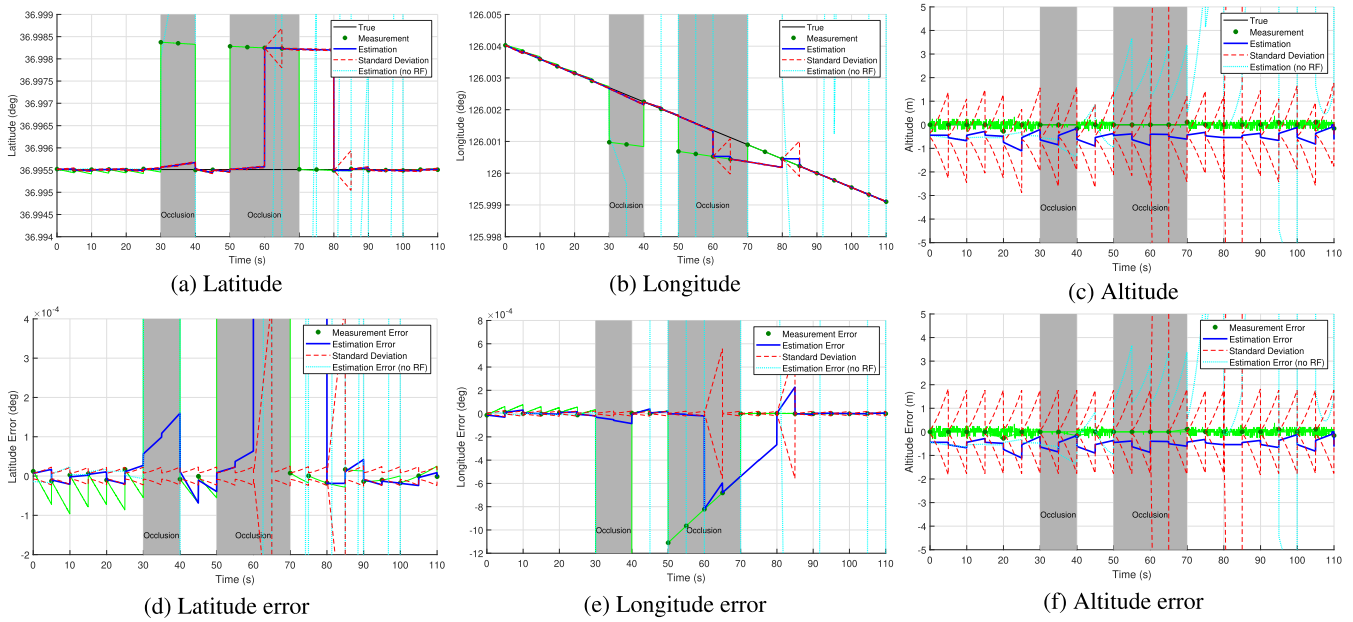


FIGURE 10. State estimator simulation result under occlusion - Outbound case.



(a) EO/IR (L3Harris Technolo-gies WESCAM MX-10MS) (b) GPS receiver (Qstarz BL-1000GT)

FIGURE 11. Sensors for the field test.

than normal Gaussian noise are not considered to compare only the estimation performances of the filters. The accuracy of the position estimation is the primary factor determining which estimation method is used as the default filter. The velocity accuracy is another important consideration, whereas the acceleration accuracy is not compared explicitly in this study. Note that the comparison results may differ depending on the scenario and the filter parameters. Some important characteristics of a scenario affecting the result are the maneuverability of the target and distance range throughout the scenario. A Monte Carlo simulation study on a single scenario does not guarantee determination of which filter is most appropriate. Moreover, a ‘best’ estimation method for a wide range of operational environments does not exist, hence the importance of the integrated framework proposed in this study.

Second, the integrated target tracker combined with an independent range filter is compared with a monolithic target tracking filter. In the hardware system considered in this study, the LRF is the only device that can experience a radical change in measurements in unexpected situations.

The azimuth and elevation measurements are more robust even when the target is not visible for a short period of time because they are based on visual target tracking. Therefore, it may be more efficient and robust to handle exceptional signal attributes by using an independent range filter instead of carrying out the whole process once using only the main filter. Target tracking simulation results with and without a range filter are shown in Figs. 9-10. Clearly, the filter without a range filter quickly diverges when the LRF does not perform properly. Moreover, once the filter diverges, the tracking performance is not recovered even after the LRF resumes providing accurate measurements. On the other hand, the proposed filter does not diverge and maintains a moderate error level during the abnormal period without compromising the tracking performance in the normal environment. Note that the range filter can also be designed according to the motion model used and that the optimal choice is dependent on the environment and the target maneuverability.

V. PERFORMANCE VERIFICATION VIA A FIELD TEST

Field tests are performed to verify the performance and effectiveness of the proposed target tracking system. A schematic diagram of the hardware system is shown in Fig. 12. A low-speed fishing boat and a multicopter drone are considered, as shown in Fig. 13a and Fig. 13b, respectively. A set of sensors is used to collect the target information. Then, the designed target tracking algorithm is implemented in the hardware for real-time target tracking. Target tracking is performed based on the predefined sequences of the operational modes designed in the previous sections.

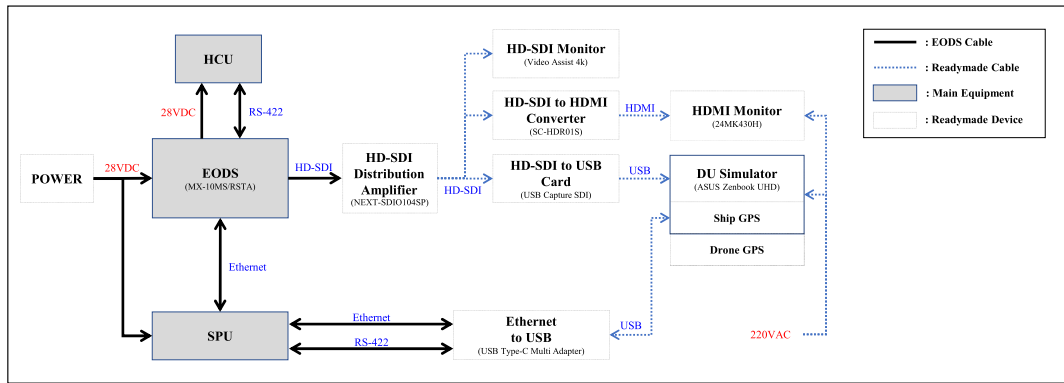


FIGURE 12. Schematic diagram of the hardware system.

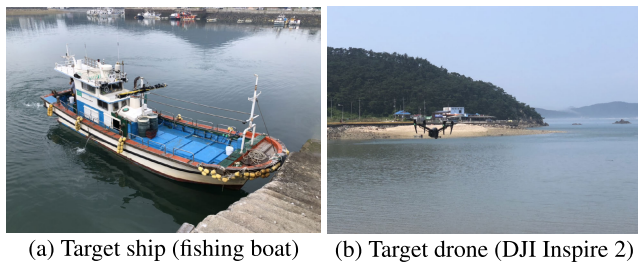


FIGURE 13. Targets for the field test.

A. SENSORS

Let us introduce the sensors used in the target tracking system. The electro-optical infrared device considered in this study is an integrated system with image sensors, infrared sensors, and an LRF. The device is mounted onto the platform, which measures the distance and direction of the target from the platform. The device used in the hardware experiment is L3Harris Technologies WESCAM MX-10MS, which is shown in Fig. 11a.

In this study, it is assumed that the image sensor always points toward the target. This assumption is justified because the software suite provides automatic video tracking (AVT) through image processing. Because the AVT provides robust target tracking, it is assumed that the sensor is always aligned with the target. Therefore, the azimuth and elevation of the target are the same as the pan and tilt angle of the gimbal. However, in the field test, this assumption may be violated by various factors such as target evasive maneuvers, vibration of the platform, and atmospheric conditions [13]. This study does not consider the situations in which a target tracking error occurs in the image plane due to the disturbances mentioned.

In the experimental test, a relative misalignment exists between the  $x - y$  plane of the platform and the floor of the electro-optical infrared sensor, which may cause significant errors in the altitude estimates of the target. A level meter is used to measure the alignment error of each axis, and a compensation algorithm is implemented to estimate the alignment error based on the measurements. The sen-

TABLE 3. Specifications of the sensors in the target tracking system.

Sensor	Parameter	Value
LRF	Resolution	1 m
	Max. range	20 km
	Frequency	0.2 Hz / 1 Hz / 5 Hz
Image sensor	Type	3-5 $\mu\text{m}$ straying array
	Resolution	640 x 512 pixels
	Field of view	30.0° to 1.8° continuous zoom
Gimbal	Resolution	0.01 deg
	Azimuth range	360 deg
	Elevation range	-90 to 110 deg
	Frequency	30 Hz
Platform GPS/INS	Position accuracy	1 m (CEP)
	Attitude accuracy	0.01 deg
	Frequency	10 Hz
Target GPS	Accuracy	3 m (CEP)
	Frequency	10 Hz

sors used in the target tracking system are described in the following.

1) LASER RANGEFINDER

The LRF measures the distance of the target from the platform. In the operational situation, the LRF may measure the distance of other objects instead of the target. In addition, laser signals reflected from the waves may degrade the target detection performance. As mentioned in the numerical simulation section, the LRF measurements in the simulation take into account the above characteristics. The detailed product specifications of the LRF are summarized in Table 3. The LRF resolution is the smallest change in distance the sensor can detect in the quantity that it is measuring.

2) ELECTRO-OPTICAL INFRARED SENSOR

The image sensor is typically used to detect, recognize, and identify the target within a limited field of view. The

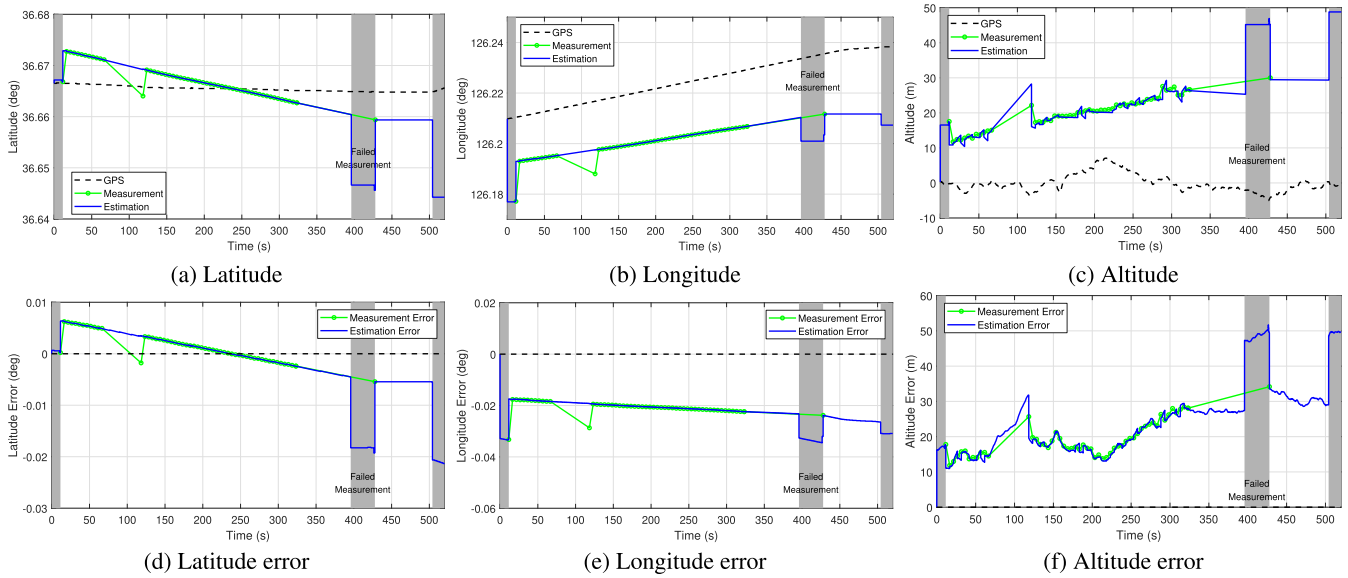


FIGURE 14. Field test results - Boat target.

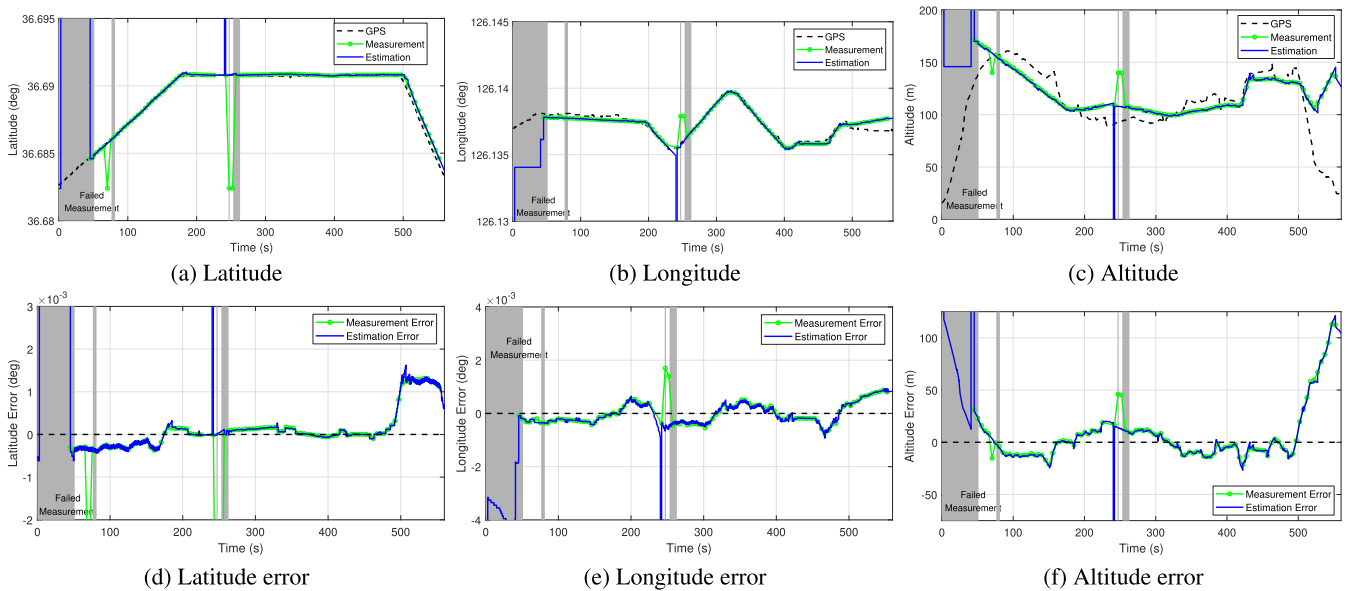


FIGURE 15. Field test results - Drone target.

electro-optical infrared (EO/IR) image sensor involves a video camera operating in the visible and infrared portions of the electromagnetic spectrum. The visible range of an image sensor benefits from the availability of color data and high-quality optics. On the other hand, IR sensors offer effective nighttime visibility. The disadvantage of image sensors is that the measurement is affected by atmospheric conditions such as weather changes, sunlight, and wakes [14].

### 3) GIMBAL

All built-in sensors are mounted on a two-axis gimbal, which has an actuated axis pan (azimuth) and tilt (elevation) to stabilize the pointing direction of the sensors. A controller is designed to follow a given azimuth and elevation com-

mand. In practice, some disturbances may cause tracking errors or jitter, such as kinematic coupling and mass imbalances [13]. Several studies have been conducted on the control law under these disturbances [15], [16].

### 4) PLATFORM GPS/INS

To locate a target in an inertial coordinate system (the ECEF coordinate system in this study), an accurate position and attitude of the platform are required. The platform GPS/INS sensor provides the position and attitude of the platform with high accuracy.

### 5) TARGET GPS RECEIVER

A GPS receiver is mounted onto the target to obtain its actual location information to verify the accuracy of the

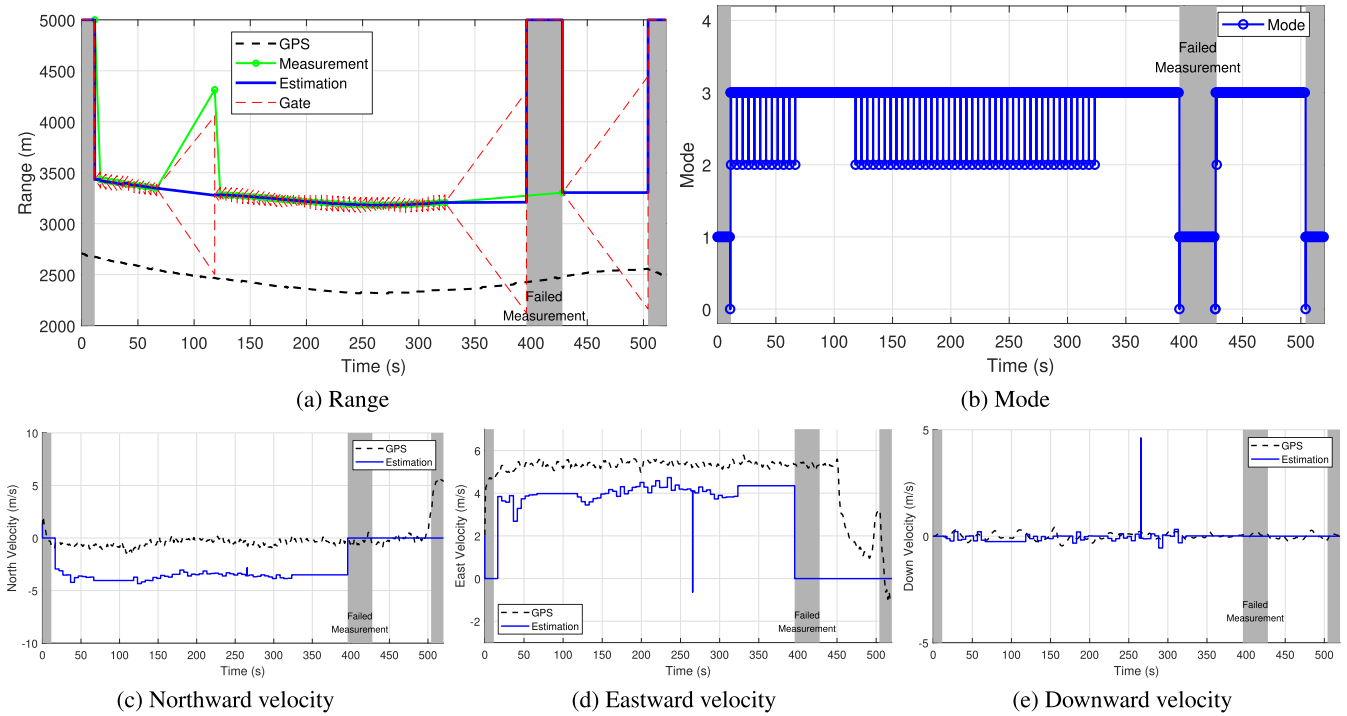


FIGURE 16. Filter state - Boat target.

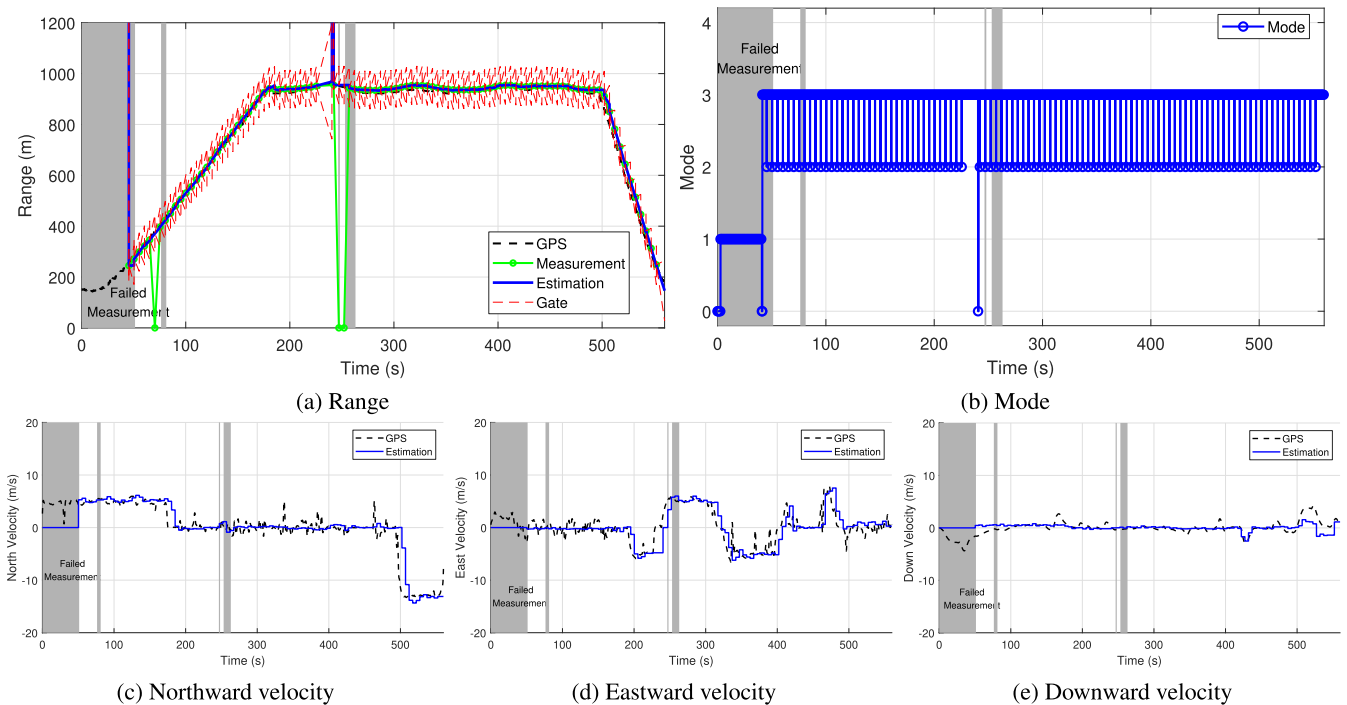


FIGURE 17. Filter state - Drone target.

designed tracking filter. The GPS receiver used in the hardware experiment is a BL-1000GT GPS racing recorder from Qstarz, as shown in Fig. 11b. The detailed product specifications of the GPS receiver are summarized in Table 3.

### B. FIELD TEST

Field tests are performed to demonstrate the effectiveness of the proposed system. The filter parameters used in the field tests are summarized in Table 4. The range filter is set to propagate the estimated range up to 20 s when no

TABLE 4. Selected filter parameters for the field test.

Range filter		State estimator	
Parameter	Value	Parameter	Value
Propagation limit	20 s	Process noise	1 m/s <sup>2</sup>
Target speed limit	15 m/s	Measurement noise (A)	0.1 deg
Process noise	10 m/s <sup>2</sup>	Measurement noise (E)	0.1 deg
Measurement noise	1 m	Measurement noise (R)	1 m

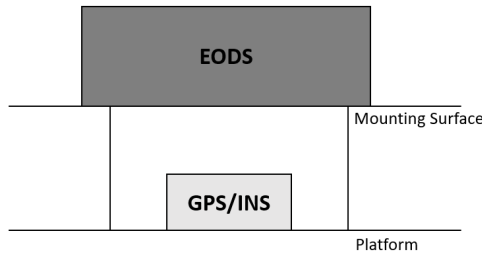


FIGURE 18. Tilted mounting surface.

valid measurement occurs for a period of time. During the propagation-only period, the gate width is continuously expanded under the assumption that the target can move in an arbitrary direction at a rate of no more than 15 m/s. Note that the process noise level of the state estimator is more conservative than that of the range filter and that the measurement noise levels are determined based on the sensor specifications. In the field test, a low-speed fishing boat (Fig. 13a) and a small drone (Fig. 13b) are considered the targets. The targets perform prescribed maneuvers within a 10 km distance from the sensor. The target tracking filter runs online, and the filter output is monitored in real time by a human operator. Furthermore, GPS receivers (Fig. 11b) are attached to the targets, and the GPS-based position and velocity are compared offline to the filter output. The GPS-based velocity is calculated by using the speed and heading. The complete setup of the hardware system for the field test is shown in Fig. 12. The equipment in the gray boxes represents the main components of target tracking, while the others are auxiliary devices for operation, monitoring, and analysis. The main equipment is installed on the ground so that the attitude of the platform is fixed throughout the test.

The first field test is performed with the boat target, one typical case of which is presented here. Figs. 14 and 16 show the measurement and estimation results. In this test, the sensor location is fixed on the ground, and the boat travels from the west to the east at 5 km/h, maintaining an approximately 3 km distance from the sensor, as shown in Fig. 16. In Fig. 14, two kinds of errors are observed. First, offset errors exist in the position estimates and the range measurement, which are due to the platform position initialization error. Second, the slopes of the GPS data and the estimates are different because of an incorrect platform attitude initialization. These

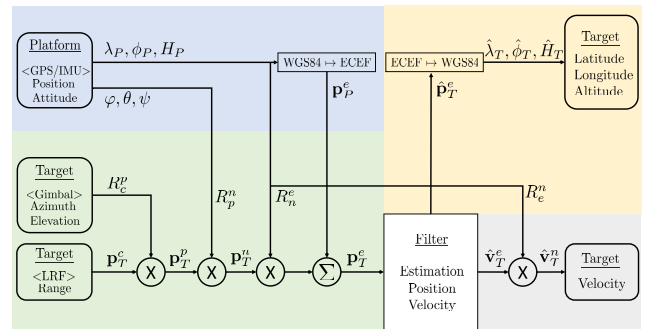


FIGURE 19. Coordinate transformation scheme.

errors can be eliminated by increasing the accuracy of the platform position and attitude initialization.

The second stage of the test is performed with a multicopter drone after precise initialization. In this stage, most of the error sources are eliminated except for the sensor misalignment. As shown in Fig. 15, the latitude, longitude, and altitude were precisely estimated. Figs. 17a and 17b show that the range filter constantly provides range estimates even under detection failure until the filter is commanded to perform a hard reset. Fig. 15c shows that meter-level altitude errors exist, but it is difficult to judge the true accuracy due to the poor altitude accuracy of the GPS data. The source of the remaining errors is considered to be the sensor misalignment. This error can be fixed by applying a simple rotation compensation algorithm using inclination measurements.

In summary, the sources of error can be divided into two types. First, systematic errors exist, most of which can be significantly reduced. The target information is computed based on the knowledge of the sensor position and attitude. Systematic errors are caused by the platform position on the Earth, platform attitude with respect to the local horizon, and relative attitude of the mounting surface with respect to the platform, as shown in Fig. 18. Second, random errors exist that are more difficult to compensate for. Every single measurement is prone to be corrupted by white Gaussian random noise. In practice, it is difficult to accurately obtain the target velocity using only a GPS receiver. Finally, some errors occur in a rather discontinuous manner. The video tracker and the LRF may fail to detect the target due to clouds, ground objects, the sun, and the target being out of range. In this study, most of the aforementioned errors are addressed, but some discrepancies still exist between the estimated and true (at least approximately) values of the target position and velocity. The errors can be further analyzed effectively by performing proper unit tests and improving the performance of the filter algorithm.

## VI. CONCLUSION

A target tracking system using a laser rangefinder was developed based on a range filter and a state estimation algorithm. General guidelines for the selection of the coordinate systems, motion models, and estimation methods were

presented. The development process was described in detail to facilitate future research of a similar nature. The performance comparison results of various state estimation methods were presented. Finally, a target tracking algorithm with the combined range filter and state estimator was designed, and the effectiveness of the proposed method was demonstrated through numerical simulations and experimental tests.

Developing a single universal target tracking system that works optimally against all kinds of targets is nearly impossible. The system presented in this study was designed to be appropriate for a single gently maneuvering target with the specified sensor combination. Some additional problems must be solved to deal with a highly maneuverable target or multiple targets, and the sensor requirements should also be changed considering the target characteristics. Nevertheless, the development process proposed in this study can be applied effectively and efficiently to a wide range of target tracking systems, and the fundamental algorithms proposed here can be utilized for various tracking systems.

## APPENDIX

This section introduces the coordinate transformation formula used in the target tracking algorithm. A schematic diagram of the coordinate transformation process is shown in Fig. 19. This section consists of four parts. Each subsection gives details about the coordinate transformation formula used in the corresponding area of Fig. 19.

### A. WGS-84 TO ECEF

To convert the position from the WGS-84 to the ECEF coordinate system, the following equations can be used.

$$x = (\rho + H) \cos \phi \cos \lambda \quad (\text{A.1})$$

$$y = (\rho + H) \cos \phi \sin \lambda \quad (\text{A.2})$$

$$z = (\rho(1 - e^2) + H) \sin \lambda \quad (\text{A.3})$$

where  $\phi$ ,  $\lambda$ , and  $H$  denote the geodetic latitude, longitude, and altitude, respectively,  $a$  and  $e$  denote the semimajor axis and eccentricity, respectively, and  $\rho = \frac{a}{1 - e^2 \sin^2 \phi}$ .

### B. ECEF TO WGS-84

The position information of the object provided by the GPS receiver is expressed in the WGS-84. To verify the performance of the tracking filter, it is necessary to convert the estimated location information from the ECEF coordinate system to the WGS-84 coordinate system to compare the estimated target position with the data from the GPS receiver mounted on the target. Three components of the ECEF coordinate system, which are represented as  $x$ ,  $y$ , and  $z$ , are converted to the geodetic latitude ( $\phi$ ), geodetic longitude ( $\lambda$ ), and altitude ( $H$ ), respectively. The geodetic longitude can be easily calculated as

$$\lambda = \tan^{-1}\left(\frac{y}{x}\right) \quad (\text{B.1})$$

The geodetic latitude and altitude are obtained from the iterative algorithm summarized in Algorithm 1.

### Algorithm 1: Geodetic Latitude and Altitude Calculation Algorithm

Given  $x$ ,  $y$ , and  $z$

Initialization;  $H \leftarrow 0$ ;  $N \leftarrow a$ ;

**while**  $\delta H > \epsilon$  **do**

$$\left[ \begin{array}{l} \phi \leftarrow \tan^{-1}\left[\frac{z}{\sqrt{x^2+y^2}}\left(1 - \frac{e^2 N}{N+H}\right)^{-1}\right] \\ N \leftarrow \frac{a}{\sqrt{1-e^2 \sin^2 \phi}} \\ H \leftarrow \frac{\sqrt{x^2+y^2}}{\cos \phi} - N \end{array} \right.$$

\* $x$ ,  $y$ , and  $z$  are the components of the position in the ECEF coordinate system, and  $a$  and  $e$  are the semimajor axis and eccentricity of the Earth, respectively.

### C. CAMERA TO ECEF

The built-in sensor of the electro-optical infrared sensor provides the azimuth and elevation information in the platform coordinate system. Moreover, the LRF in the EO/IR device provides the range information. Thus, a coordinate transformation is required to obtain the target information in the ECEF coordinate system. The detailed conversion process is as follows.

#### 1) CAMERA TO PLATFORM

The location of the target in the platform coordinate system is determined from the geometric relationship shown in Fig. 1c as

$$\mathbf{p}_T^p = \begin{bmatrix} R \cos E \cos A \\ R \cos E \sin A \\ R \sin E \end{bmatrix} \quad (\text{C.1})$$

where  $\mathbf{p}_T^p$  is the position of the target in the platform coordinate system and  $R$ ,  $E$ , and  $A$  denote the range, elevation, and azimuth of the target, respectively. A difference exists between the position of the attitude sensor (center of the measurement device) and that of the platform. Generally, the effect of this difference on the accuracy of the sensor is negligible.

#### 2) PLATFORM TO NAVIGATION

The attitude information of the platform (roll, pitch, and yaw angles) can be accurately estimated from the embedded GPS/INS measurements. With the platform Euler angles, the coordinates can be converted from the navigation coordinate system to the platform coordinate system through the 3-2-1 Euler transformation as

$$R_n^p = \begin{bmatrix} 1 & 0 & 0 \\ 0 & \cos \varphi & \sin \varphi \\ 0 & -\sin \varphi & \cos \varphi \end{bmatrix}$$

$$\begin{bmatrix} \cos \theta & 0 & -\sin \theta \\ 0 & 1 & 0 \\ \sin \theta & 0 & \cos \theta \end{bmatrix} \begin{bmatrix} \cos \psi & \sin \psi & 0 \\ -\sin \psi & \cos \psi & 0 \\ 0 & 0 & 1 \end{bmatrix} \quad (C.2)$$

where  $R_n^p$  is a direction cosine matrix from the navigation to the platform coordinate system and  $\varphi$ ,  $\theta$ , and  $\psi$  are the roll, pitch, and yaw angles of the platform, respectively. The direction cosine matrix from the platform to the navigation coordinate transformation can be obtained by transposing  $R_n^p$  as

$$R_p^n = (R_n^p)^T \quad (C.3)$$

Thus, the coordinate transformation from the platform to the navigation coordinate system can be expressed in the following equation as

$$\mathbf{p}_T^n = R_p^n \mathbf{p}_T^p \quad (C.4)$$

where  $\mathbf{p}_T^n$  and  $\mathbf{p}_T^p$  are the positions of the target with respect to the navigation and platform coordinate systems, respectively.

### 3) NAVIGATION TO ECEF

The platform latitude and longitude are required to obtain the position of the target in the ECEF coordinate system. The direction cosine matrix can be expressed as

$$R_e^n = \begin{bmatrix} \cos(\pi/2 + \phi_P) & 0 & -\sin(\pi/2 + \phi_P) \\ 0 & 1 & 0 \\ \sin(\pi/2 + \phi_P) & 0 & \cos(\pi/2 + \phi_P) \end{bmatrix} \quad (C.5)$$

$$R_n^e = (R_e^n)^T \quad (C.6)$$

where  $\phi_P$  and  $\lambda_P$  denote the geodetic latitude and longitude, respectively.

The position of the target in the ECEF coordinate system can be obtained by

$$\mathbf{p}_T^e = R_n^e \mathbf{p}_T^n + \mathbf{p}_P^e \quad (C.7)$$

where  $\mathbf{p}_T^e$  and  $\mathbf{p}_P^e$  denote the positions of the target and platform in the ECEF coordinate system, respectively.

### D. ECEF TO NAVIGATION

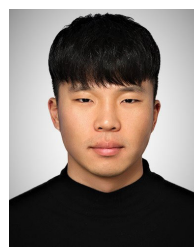
In this study, the estimated target velocity is compared with GPS receiver data in the navigation coordinate system. The target velocity in the ECEF coordinate system is converted to the navigation coordinate system by

$$\mathbf{v}_T^n = R_n^e \mathbf{v}_T^e \quad (D.1)$$

where  $\mathbf{v}_T^n$  and  $\mathbf{v}_T^e$  denote the target velocity in the navigation and ECEF coordinate systems, respectively.

### REFERENCES

- [1] V.-D. Hoang and K.-H. Jo, "A simplified solution to motion estimation using an omnidirectional camera and a 2-D LRF sensor," *IEEE Trans. Ind. Informat.*, vol. 12, no. 3, pp. 1064–1073, Jun. 2016.
- [2] E.-J. Jung, J. H. Lee, B.-J. Yi, J. Park, S. Yuta, and S.-T. Noh, "Development of a laser-range-finder-based human tracking and control algorithm for a marathoner service robot," *IEEE/ASME Trans. Mechatronics*, vol. 19, no. 6, pp. 1963–1976, Dec. 2014.
- [3] H. Kaushal and G. Kaddoum, "Applications of lasers for tactical military operations," *IEEE Access*, vol. 5, pp. 20736–20753, Sep. 2017.
- [4] K. Dai, Y. Wang, J.-S. Hu, K. Nam, and C. Yin, "Intertarget occlusion handling in multiextended target tracking based on labeled multi-Bernoulli filter using laser range finder," *IEEE/ASME Trans. Mechatronics*, vol. 25, no. 4, pp. 1719–1728, Aug. 2020.
- [5] H. Wei, Z.-P. Cai, B. Tang, and Z.-X. Yu, "Review of the algorithms for radar single target tracking," *IOP Conf. Ser., Earth Environ. Sci.*, vol. 69, May 2017, Art. no. 012073.
- [6] K. Saho and M. Masugi, "Performance analysis of  $\alpha$ - $\beta$ - $\gamma$  tracking filters using position and velocity measurements," *EURASIP J. Adv. Signal Process.*, vol. 2015, no. 35, pp. 1–15, Dec. 2015.
- [7] X. R. Li and V. P. Jilkov, "Survey of maneuvering target tracking: III. Measurement models," *Proc. SPIE*, vol. 4473, pp. 423–446, Nov. 2001.
- [8] P. R. Mahapatra and K. Mehrotra, "Mixed coordinate tracking of generalized maneuvering targets using acceleration and jerk models," *IEEE Trans. Aerosp. Electron. Syst.*, vol. 36, no. 3, pp. 992–1000, Jul. 2000.
- [9] T. L. Song, J. Y. Ahn, and C. Park, "Suboptimal filter design with pseudomeasurements for target tracking," *IEEE Trans. Aerosp. Electron. Syst.*, vol. AES-24, no. 1, pp. 28–39, Jan. 1988.
- [10] V. Aidala and S. Hammel, "Utilization of modified polar coordinates for bearings-only tracking," *IEEE Trans. Autom. Control*, vol. AC-28, no. 3, pp. 283–294, Mar. 1983.
- [11] R. Yanushevsky, *Modern Missile Guidance*, 2nd ed. Boca Raton, FL, USA: CRC Press, 2018.
- [12] J. E. Gray and W. Murray, "A derivation of an analytic expression for the tracking index for the alpha-beta-gamma filter," *IEEE Trans. Aerosp. Electron. Syst.*, vol. 29, no. 3, pp. 1064–1065, Jul. 1993.
- [13] M. K. Masten, "Inertially stabilized platforms for optical imaging systems: Tracking dynamics target with mobile sensors," *IEEE Control Syst. Mag.*, vol. 28, no. 1, pp. 47–64, Feb. 2008.
- [14] D. K. Prasad, D. Rajan, L. Rachmawati, E. Rajabally, and C. Quek, "Video processing from electro-optical sensors for object detection and tracking in a maritime environment: A survey," *IEEE Trans. Intell. Transp. Syst.*, vol. 18, no. 8, pp. 1993–2016, Aug. 2017.
- [15] B. Li, D. Hullender, and M. DiRenzo, "Nonlinear induced disturbance rejection in inertial stabilization systems," *IEEE Trans. Control Syst. Technol.*, vol. 6, no. 3, pp. 421–427, May 1998.
- [16] M. M. Abdo, A. R. Vali, A. R. Toloei, and M. R. Arvan, "Stabilization loop of a two axes gimbal system using self-tuning PID type fuzzy controller," *ISA Trans.*, vol. 53, no. 2, pp. 591–602, Mar. 2014.



**JIHOON LEE** received the B.S. degree in mechanical engineering and astronomy from Yonsei University, Seoul, South Korea, in 2014. He is currently pursuing the Ph.D. degree in aerospace engineering with Seoul National University, Seoul. His current research interests include design of target tracking systems, robust and gain-scheduled control of linear parameter-varying systems, and intelligent flight control systems for morphing aircraft.





**SUWON LEE** received the B.S. degree in mechanical and aerospace engineering from Seoul National University, South Korea, in 2015, where he is currently pursuing the Ph.D. degree. His current research interests include a path-planning algorithm for aerial vehicles and guidance laws for missiles.



**YONGJUN HEO** received the B.S. degree in software engineering from Dongguk University, South Korea, in 2003. He is currently a Research Engineer with the Weapon Integration Team, LIG Nex1 Company Ltd. His current research interests include the design of the electro-optical phase and the management of guided rocket programs.



**YOUNGJUN LEE** received the B.S. degree in mechanical and aerospace engineering from Seoul National University, South Korea, in 2019, where he is currently pursuing the Ph.D. degree in aerospace engineering. His current research interests include control theory for unmanned aerial vehicles and guidance laws for missiles.



control system design, path

**YODAN KIM** (Senior Member, IEEE) received the B.S. and M.S. degrees in aeronautical engineering from Seoul National University, South Korea, in 1983 and 1985, respectively, and the Ph.D. degree in aerospace engineering from Texas A&M University, in 1990. He joined the Faculty of Seoul National University, in 1992, where he is currently a Professor with the Department of Aerospace Engineering. His current research interests include aircraft control system design, reconfigurable control system design, path planning, and guidance techniques for aerospace systems.



**TAEDONG YOON** received the B.S. degree in industrial engineering from Kyunghee University, South Korea, in 2005. He is currently a Research Engineer with the Weapon Integration Team, LIG Nex1 Company Ltd. His current research interests include ILS development of a guided rocket and system engineering and integration of guided rocket projects.

...